Phenomenological and Global Optimization Inversion

Peter Gerstoft, *Member, IEEE*, William S. Hodgkiss, *Member, IEEE*, William A. Kuperman, and Heechun Song, *Member, IEEE*

***Abstract*—This paper discusses geoacoustic inversion results based on benchmark range-dependent data using SAGA, a global inversion package, and using phenomenological inversions. In phenomenological inversions, physical and signal-processing approaches are used to enhance the data to extract specific features. The global optimization approach is carried out on complex-valued vertical array data, transmission loss data, and reverberation data. The importance of checking the solution is emphasized by inspecting the match with the data and the error estimates and by checking the solution using data that has not been used in constructing the solution. The results show that we are able to estimate the geoacoustic parameters and that these parameters could be used to predict the field for different frequencies and/or source-receiver geometry than used in the inversion.**

***Index Terms*—Genetic algorithms (GAs), geoacoustic inversion, SAGA.**

I. Introduction

IN THIS PAPER, we use genetic algorithms (GAs) to solve several range-dependent benchmark cases [1]. A major emphasis is on understanding and accessing the inverse solution. Test Cases 0–3 (TC0–TC3) of the benchmarks involved synthetically generated data based on environments with geometries, as shown in Fig. 1. TC0 is a calibration test case with known environment. TC1 represents downslope propagation with the bathymetry ranging from 90 m (0-km range) to 150 m (5-km range). TC2 represents a shelf break with upslope bottom bathymetry changing from 140 m (0-km range) to 105 m (2.1-km to 5-km range). TC3 has a flat bottom at 100-m depth. The ocean sound speed profile is downward refracting and is given by $v = 1495 - 0.4z$, where z is the water depth in m. The source depth (SD) is 20 m. The data was generated by the fidelity parabolic equation RAMGEO code [2]. There was no uncertainty in recording geometry and both amplitude and phase were provided at multiple frequencies (25–200 Hz in 1-Hz steps and 200–500 Hz in 5-Hz steps) at two horizontal arrays (HA) at 20- and 85-m depth (hydrophone ranges 0.005–5 km in 5- m steps) and 10 vertical arrays (VA) at ranges 0.5–5 km with 0.5-km separations (hydrophone depths 20–80 m in 1-m increments).

Test Cases 4 and 5 were real data from drifting sonobuoys consisting of amplitude-only reverberation and incoherent transmission-loss data with a large uncertainty in recording geometry. Test Case 3 proved most interesting. It was only given that there was an intrusion in the sediment; there was no indication of the shape. In general, this would call for a range-dependent inversion [3] or a shape-reconstruction approach, e.g., [4] and [5]. The recording geometry for the present case is not well suited for a shape-reconstruction approach, as the source and receiver should pass over the object. In Section III, we examine which physical and signal-processing approach is best able to provide information about the intrusion.

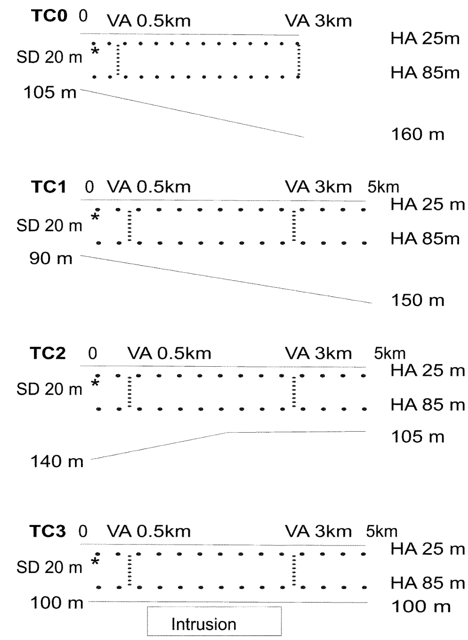

Fig. 1. Environment for TC0–TC3 indicating sloping seafloor in TC0–TC2 and intrusion in TC3. Only the recording geometry mainly used is indicated.

Test Cases 1–5 (TC1–TC5) were solved using the standard inversion package SAGA [6], [7]; see Section II. SAGA is a software package that helps the user to determine the best set of parameters to match a given data set. SAGA has integrated some of the best ocean acoustic and electromagnetic forward codes (such as SNAP [8], OASES [9], POPP [10], PROSIM [11], RAMGEO [2], ORCA [12], GAMA [13], and TPEM [14]) into the inversion and can handle many types of data, as documented in papers. As its main thrust, it uses GA, but also can handle simulated annealing, very fast simulated annealing, and Cramer–Rao bounds and Gibbs sampling of the *posteriori* probabilities. To demonstrate the versatility of SAGA, we focus on vertical complex-valued array data, transmission-loss data, and reverberation data.

II. Global Inversion of Test Cases

A. Search Method

Here, the basic search method in SAGA [6] (GAs [7], [15]), is used. Simulated annealing [16]–[18] could likely be used

Manuscript received June 17, 2002; revised November 26, 2002. This work was supported by the Office of Naval Research Code 32.

The authors are with the Marine Physical Laboratory, University of California—San Diego, La Jolla, CA 92093-0238 USA (e-mail: gerstoft@mpl.ucsd.edu).

Digital Object Identifier 10.1109/JOE.2003.816681

0364-9059/03$17.00 © 2003 IEEE

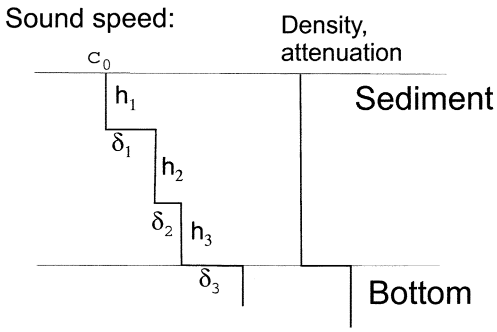

Fig. 2. Bottom environmental model. The model follows the bottom bathymetry.

TABLE I
GA Inversion Model With Parameter Search Bounds. Each Parameter was Discretized Into 128 Values

Model parameter	Lower bound	Upper bound
Sediment		
sound speed, c_0 (m/s)	1480	1600
sound speed, δ_1 (m/s)	0	250
sound speed, δ_2 (m/s)	0	150
thickness, h_1	1	10
thickness, h_2	1	20
thickness, h_3 (m)	1	30
attenuation (dB/λ)	0.01	0.5
density (g/cm^3)	1.2	1.8
Bottom		
sound speed, δ_3 (m/s)	10	400
attenuation (dB/λ)	0.01	0.2
density (g/cm^3)	1.6	2.4

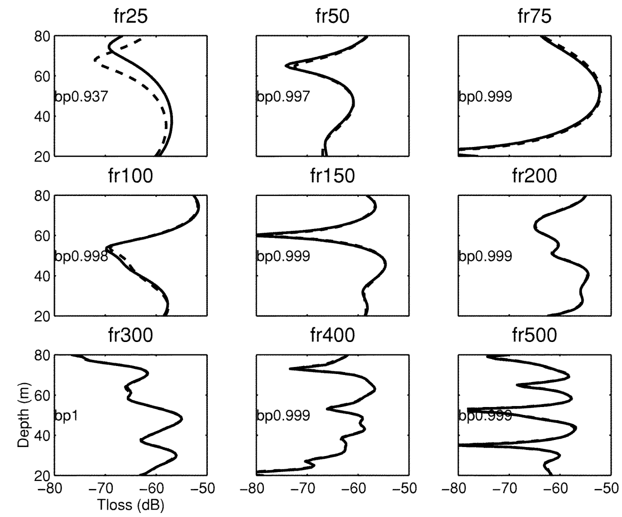

Fig. 3. Transmission loss for data (solid lines) and replica (dashed lines) for the TC0 at the vertical array at 3-km range and different frequencies. Only below 200 Hz is the difference in the fields visible. The Bartlett power for each frequency is also indicated.

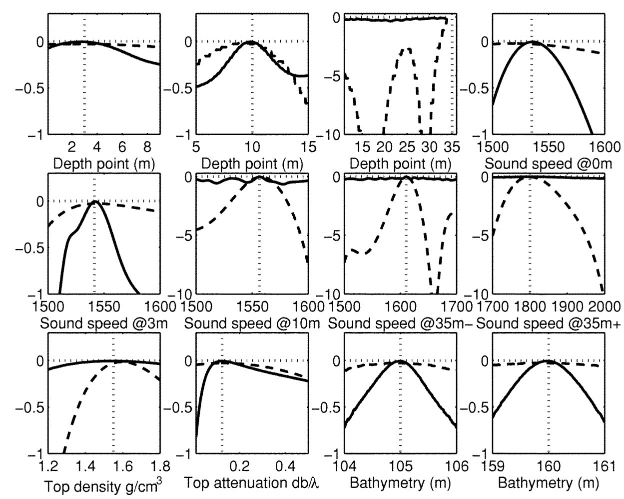

Fig. 4. Sensitivity of TC0 at 50 (dashed lines) and 500 (solid lines) Hz for the array at 3 km. One variable is perturbed at the time and all other variables are at their nominal value (vertical dotted line). The vertical axis is value of the objective function, (2), expressed in decibels and normalized so that the baseline environment has a match of 0 dB (horizontal dotted line).

with the same efficiency, especially if combined with the parameter-rotation approach of Collins and Fishman [19]. The reason for this is that simulated annealing usually is perturbed along the axis of each parameter. The parameter rotation can also be implemented for GA, but is of less importance as the perturbations are not restricted to lie along the axis [20].

Global methods are good at finding solutions in the neighborhood of the optimum solution, but local methods are much better at finding the exact value of the minima. The variance in geoacoustic estimates can be reduced by applying a local method as a final step in an optimization procedure [21]. For synthetic data with no noise and a finite number of parameterizations, the value of the combination of a global method with a local method is particularly important. But, for real data, this is of less concern. In ocean acoustics, the combination of a local method with a global method was first done in [22] using analytic derivatives based on the OASES program [9]. Potty *et al.* [23] also combined a local and a global method, but used a different objective function for the local method, which enabled them to use analytic derivatives. Finally, many authors have used the simplex method, e.g., [21] and [24]–[26]. The advantage of the simplex method is that it does not require any derivative and, thus, is easily implemented.

B. Objective Function

SAGA uses a set of objective functions derived from likelihood functions that are based on simple Gaussian assumptions [27], [28]. For the data analyzed here, we use two of these objective functions. They assume the error to be additive and identically distributed on each hydrophone, but the error level may vary across frequencies. The Gaussian assumption is related to all errors in the experiment as noise in the data, error in discretizing the environment, theoretical errors, and errors in the forward model.

For magnitude-only data (e.g., transmission-loss data and reverberation data), a simple least squares objective function is

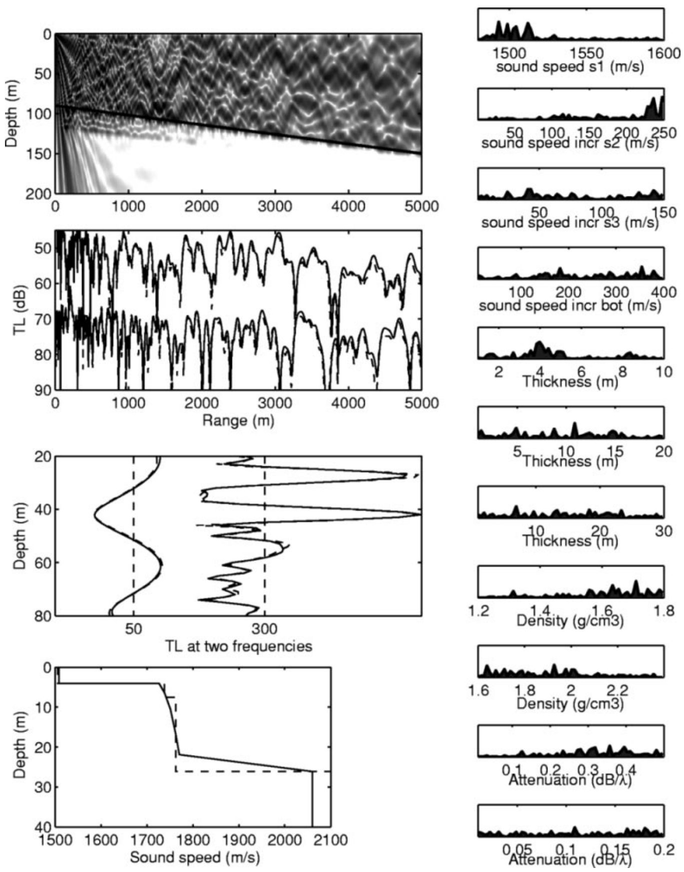

Fig. 5. Inversion display for TC1 using vertical array data at 0.5 km.

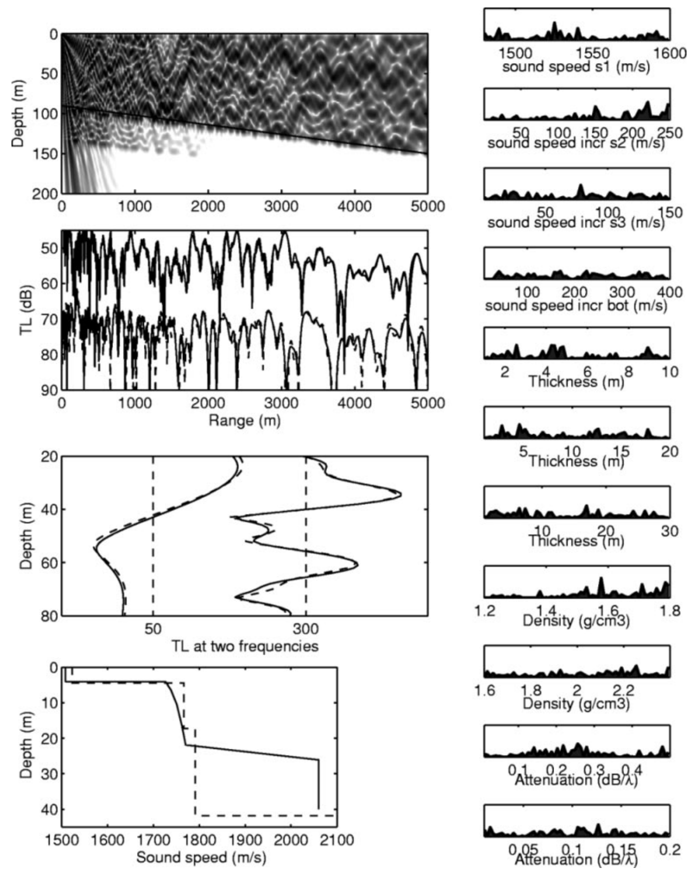

Fig. 6. Inversion display for TC1 using vertical array data at 3 km.

used between the array of N observed data values $|\mathbf{q}_l|$ and the corresponding replica $|\mathbf{w}_l(\mathbf{m})|$ at each frequency ω_l[1]

$$\phi_{l,s} = \|(|\mathbf{w}_l(\mathbf{m})| - |\mathbf{q}_l|)\|^2. \tag{1}$$

Similarly, for complex-valued data (e.g., vertical array data), an objective function related to a simple Bartlett objective function is used as follows:

$$\phi_{l,b} = \|\mathbf{q}_l\|^2 - \frac{\|\mathbf{w}_l(\mathbf{m})^\dagger \mathbf{q}_l\|^2}{\|\mathbf{w}_l(\mathbf{m})\|^2}. \tag{2}$$

Both formulations can be derived from the assumptions above and the corresponding likelihood function is

$$L_l = (2\pi\nu_l)^{-N} \exp\left[-\frac{\phi_l}{\nu_l}\right] \tag{3}$$

where ν_l is the error. In the above equation, the error is unknown and must be estimated in order to evaluate the likelihood function. The maximum likelihood approach to this is to solve $\partial L/\partial \nu_l = 0$ [27], [29]. This gives the ML estimate

$$\nu_l = \frac{1}{N_e}\phi_l(\mathbf{m}) \tag{4}$$

where the number of hydrophones N has been replaced by the effective number of hydrophones N_e [27]. At high signal-to-noise ratio (SNR) it is expected that the main error contribution is due to inadequate forward modeling. Further, the number of uncorrelated hydrophones is approximately the same as the

[1] $\mathbf{q}^\dagger$ is the Hermitian transpose of vector $\mathbf{q}$. $|\mathbf{q}|$ is the vector composed of the magnitudes of the elements of $\mathbf{q}$. $\|\mathbf{q}\|$ is the two norm of vector $\mathbf{q}$, i.e., $\sqrt{\mathbf{q}^\dagger\mathbf{q}}$.

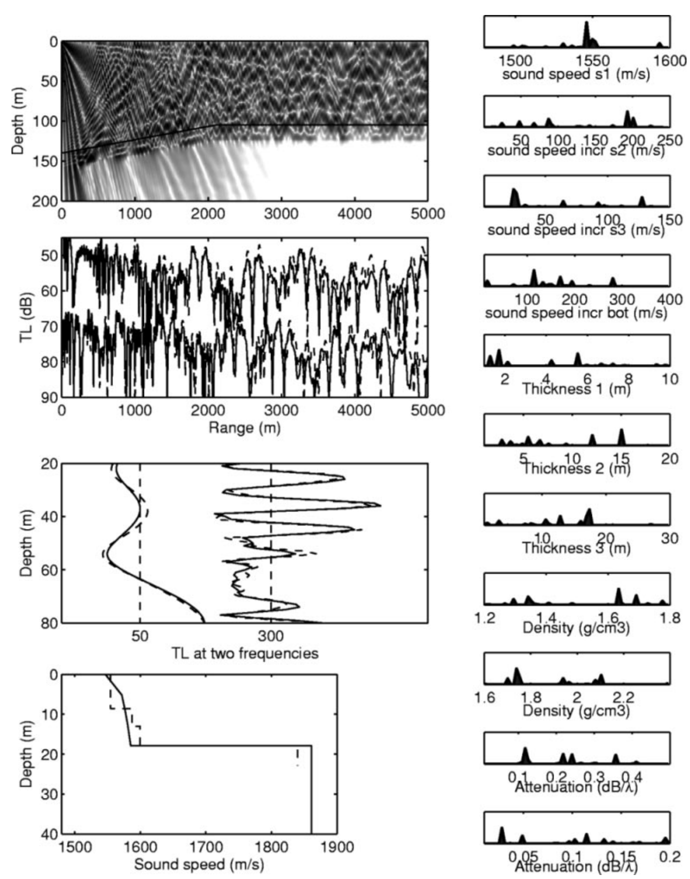

Fig. 7. Inversion display for TC2 using vertical array data at 0.5 km.

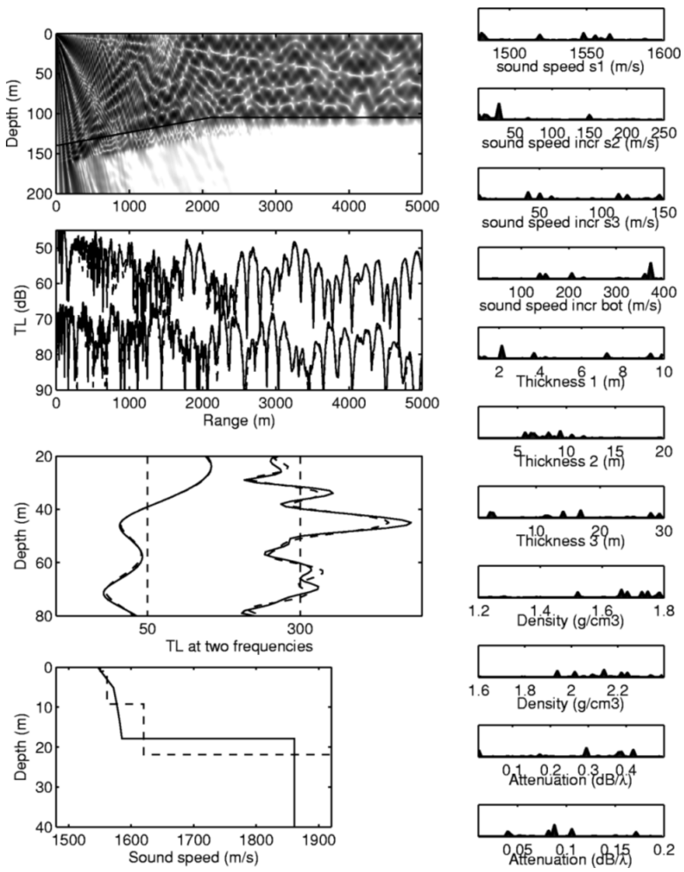

Fig. 8. Inversion display for TC2 using vertical array data at 3 km.

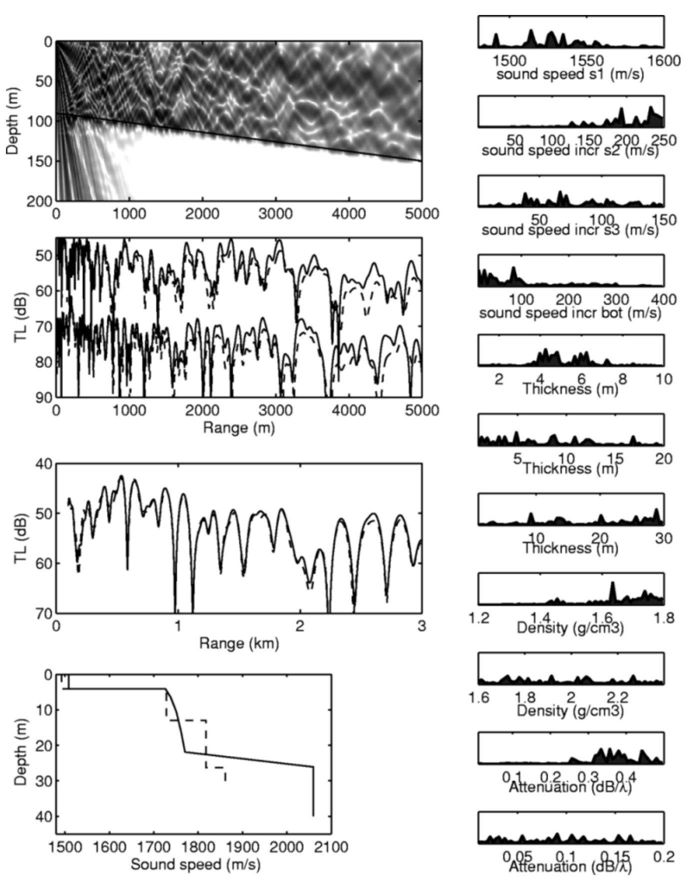

Fig. 9. Inversion display for TC1 using TL data at 85-m depth and 100 Hz.

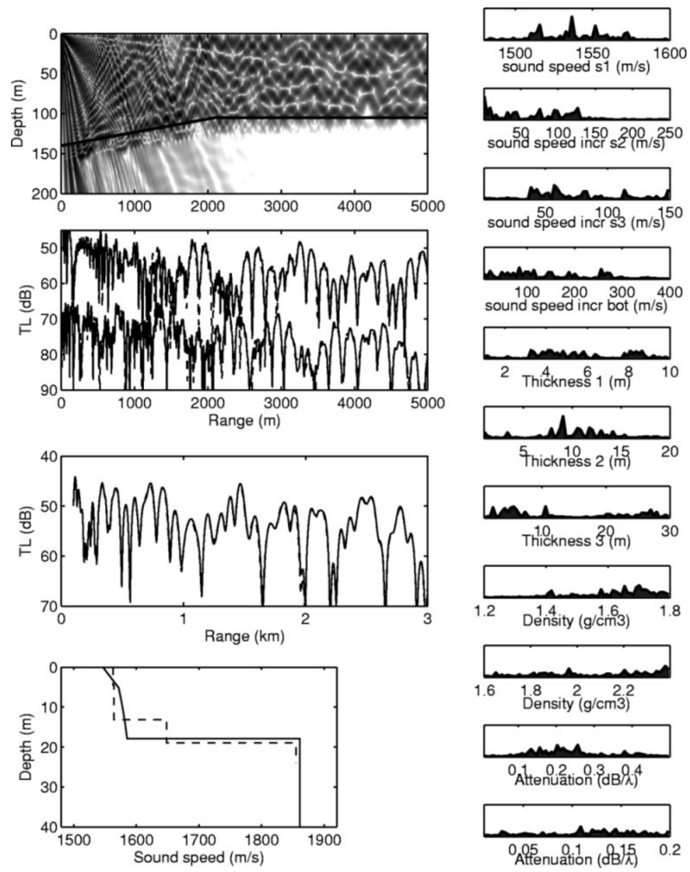

Fig. 10. Inversion display for TC2 using TL data at 85-m depth and 100 Hz.

number of propagating modes, because this limits the degrees of freedom in the random part of the acoustic wave field. The number of uncorrelated hydrophones N_e is estimated as the rank (principle component analysis) of the covariance matrix.

Multiple frequencies are combined by assuming the frequencies independent whereby the likelihood becomes

$$L = \prod L_l. \tag{5}$$

If the noise is assumed unknown and frequency dependent, then the objective function is given by [27]

$$\phi = \prod \phi_l. \tag{6}$$

The solution to the inverse problem is taken as the parameters corresponding to the optimum of the objective function, i.e., a maximum likelihood approach.

C. A Posteriori Analysis

This is one of the most important steps in an inversion approach. The optimization procedure will always determine an optimized model, but only small checks can assure that the optimized model is correct. Some useful checks are the following.

1) Objective Function: The value of the objective function should be compared to other inversion results, checked against a Chi-square test or similar.

2) Checking the Parameter Values: The obtained parameter estimates should be physically realistic. For example, use of the Hamilton relations could be used as a check [30].

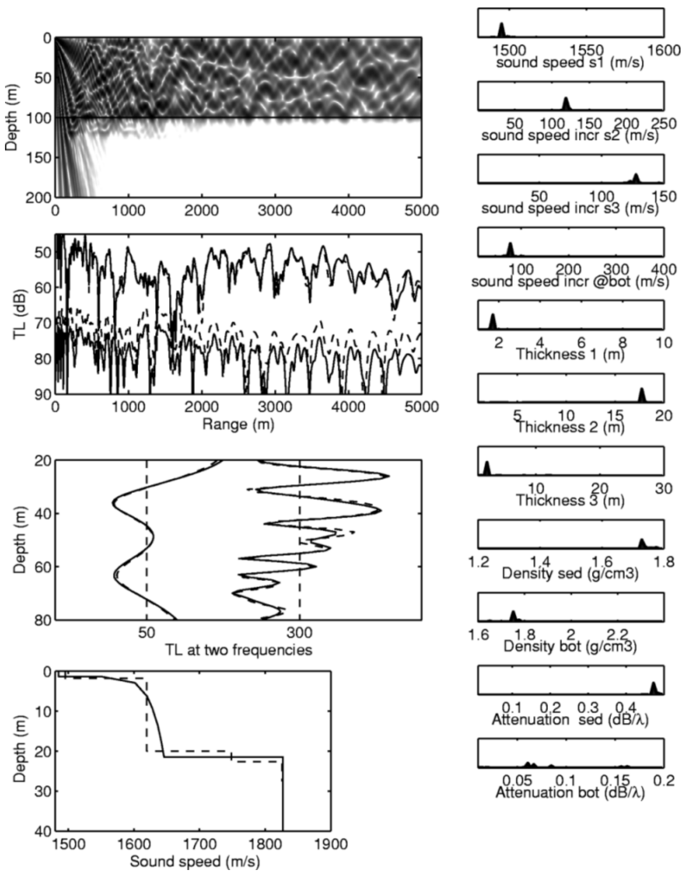

Fig. 11. Inversion display for TC3 using vertical array data at 0.5 km. The parameter estimates refers to the reference environment without the intrusion.

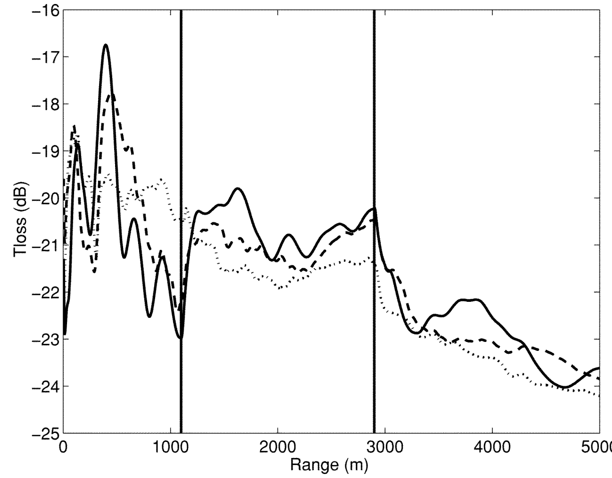

Fig. 12. Frequency-averaged 2-D transmission loss for TC3 for 25–200 Hz (dotted line), 25–100 Hz (dashed line), and 25–50 Hz (solid line).

3) Plotting the Fields: The first assessment of the quality of the inverse solution should be to plot the field generated by the inverse model and the data. This has several purposes: to find simple errors in the data (i.e., phase and magnitude errors), to find simple errors in the environmental and forward model, and to assess whether or not the essential physics is captured by the objective function.

4) Comparing the Data and Replica in a Different Domain: A good indication of how well the optimized environmental model works can be obtained by comparing the data and model using data not used previously in the inversion. For the present inversion, this is done by comparing the transmission loss at 250 Hz.

5) A Posteriori Probability Distributions: Finally, we must assess the quality of the inversions. This often is done in a Bayesian setting [7], [27], [31], estimating *a posteriori* probability distributions. This is the product of the likelihood function and the *a priori* probability distribution. Often, in ocean acoustics the *a priori* distribution is flat relative to the likelihood function and can be neglected (*a priori* probability was used in [27], but did not influence the *a posteriori* solution much). From this *a posteriori* probability distribution, all important features, such as standard deviations and one–dimensional (1-D) and two–dimensional (2-D) marginal distributions, can be estimated. Here, we focus on the 1-D marginal distributions. This corresponds to evaluating $M-1$ dimensional integrals (M is the number of parameters in the environmental model $\mathbf{m}$) of the likelihood function given in (3)

$$p(m_i) = \int L(\mathbf{m}')\delta(m_i' - m_i)d\mathbf{m}' \tag{7}$$

where δ is the Dirac delta function. As discussed in [27] and [31], the way to estimate these distributions is through importance sampling of the $M-1$ dimensional integral. This should be done using Gibbs sampling as an unknown bias otherwise will be introduced. The distribution can be interpreted as likelihood-weighted histograms of the obtained samples.

In the present case, all of the model samples from the GA optimization run are used to estimate the marginal probability density functions; the value for each parameter was binned into 64 bins. This is not as accurate as using the Fast Gibbs Sampler of Dosso [31], [32].

D. Environmental Model

The environmental model $\mathbf{m}$ for the bottom was unknown. Some range dependence was expected in the environment, as the cases were known to be range dependent with range-dependent bathymetry. A simple model would just let the sediment layers be parallel to the sea-bed layers with constant properties in each layer. A more complicated range dependence would be to let the parameters in each layer be range (or sector) dependent [3]. If the true environment was range dependent, then a range independent inversion would introduce an unknown bias [33].

Initial analysis attempted to detect range dependence: trial runs, physical inspection, and hypothesis testing [34] were also used in this initial step. The goal of this step is to determine if the parameterization is consistent with the resolution of the acoustic data. An initial attempt to automate this is presented in [26].

Finally for TC1–TC3, a three-layer sediment with a constant, but unknown, density and attenuation in the sediment, on top of a halfspace was used as an environmental model (see Fig. 2) with search bounds as indicated in Table I. In each sediment layer, the thickness h_i and sound speed increase δ_i are unknown. In the bottom layer, the sound speed, density, and attenuation are unknown. Thus, the sound speed profile is described using seven

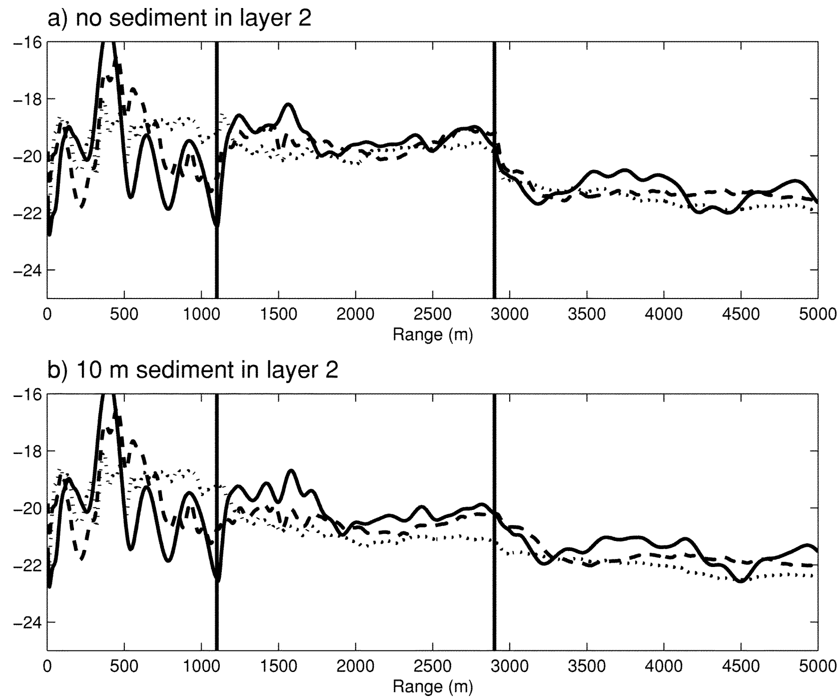

Fig. 13. Simulation of the frequency-averaged TL for 25–200 Hz (dotted line), 25–100 Hz (dashed line), and 25–50 Hz (solid line) for (a) no sediment layer and (b) a 10-m sediment layer.

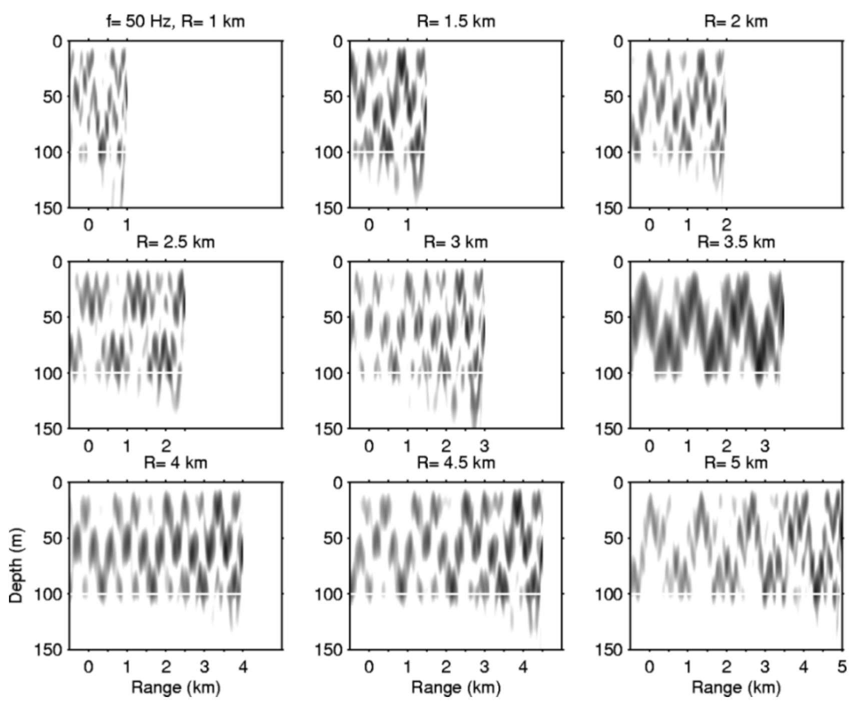

Fig. 14. Back-propagated field (dB) from each of the nine vertical arrays at range 1–5 km using the 50-Hz data. The arrows indicate locations of secondary sources in the bottom due to inhomogeneities. The dynamic range is 10 dB. The level in the bottom is magnified 1 dB/m in order to display the weak signal.

parameters (four for sound speed and three for thickness). The search interval for each δ_i is constrained to positive values, constraining the sound speed profile to be increasing. Both attenuation and density are described with two parameters. For real data inversion, this model is likely too complicated and should be simplified, as it is not possible to estimate all parameters well. For the present noise-free data, it would probably have been beneficial to use an even more complicated bottom that also included gradients in each of the three layers.

E. The Data

The supplied data for TC0–TC3 were generated synthetically using the RAMGEO PE propagation code [2]. For the calibration case, TC0, the environment was known and was used to

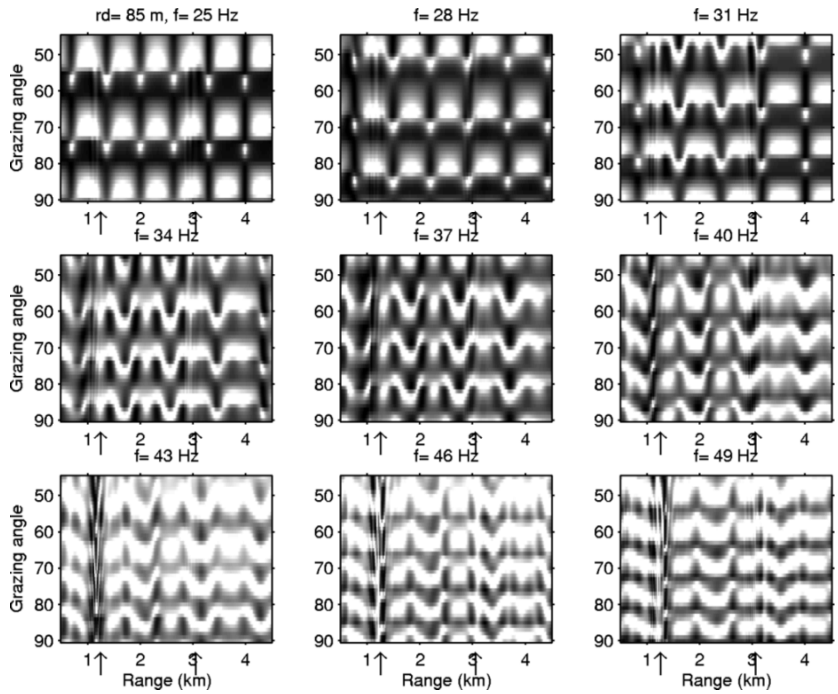

Fig. 15. Beamforming on a 200-m horizontal array at 85-m depth using the 25–49 Hz data. The arrows indicate changes in the response due to changes in the environment.

check the difference between the RAMGEO installation for the data generation and our installation at the Marine Physical Laboratory (see Fig. 3) where the response at the array at 3-km range is computed at several frequencies. Even though the input model is the same, considerable differences exist in the field, especially at low frequencies. (Later analysis ascribes this error to differences in the vertical discretization between the supplied and modeled data. This difference can be eliminated using a double-precision version of RAMGEO [35]. This was not done here. However, SAGA does now always use RAMGEO in double precision.) Thus, we cannot expect to retrieve the parameters exactly and data below 50 Hz will not be used.

In real data inversions, more frequencies usually give better estimates. For the present, noise-free synthetic inversions, data at only a few frequencies are sufficient for obtaining good inversion results. At short ranges, data from all frequencies penetrate into the bottom, but higher frequencies have a higher resolution of the bottom. For larger ranges, the field will usually see a few wavelengths into the bottom. Thus, a low frequency will see deeper than a high frequency, but the high frequency should resolve the top sound speed better. For both the 0.5- and 3-km array, data at 50 and 300 Hz are used simultaneously. For transmission-loss data, both near- and farfield data are captured; thus, data at just one frequency (100 Hz) were used. It should be noted that, for real data inversion, use of data at several frequencies often provides better results.

F. Parameterization

Indications of the sensitivity for each parameter are obtained by doing local perturbations for one parameter at a time (see Fig. 4). Here, 0 dB corresponds to the match using the reference environment. Because of difference in the RAMGEO installations used here and the one that has generated the data, the best match might not be at the reference value and the fit at that point might not be 0 dB. This mostly occurs for the 50-Hz data (see Section II-E), indicating a larger mismatch for lower frequencies. Because of deeper penetration, the lower frequencies are more sensitive to the sound speed profile deeper in the sediment and the higher frequencies are more sensitive to parameters near the seabottom (top sound speed in sediment, bathymetry).

A simple sensitivity study gives a good indication of the sensitivity of each parameter. Because this represents only a line cut through a multidimensional surface, the results should be interpreted with care.

G. Test Cases

The basic environments are shown in Fig. 1. Apart from the change in bathymetry, the same environment was used for each of the cases, inverting for the same parameters. Thus, it is not labor demanding to prepare the inversions. During the inversion, a display similar to Figs. 5–10 was updated continuously and the quality of the inversion can then be assessed before the inversion has finished.

The display shows: *(top)* A contour plot of the TL (decibels) for the best matching field, which is useful for understanding the solution. All TL has be corrected for cylindrical spreading by adding $10\log(R)$. *(left, upper middle)* Comparison of observed TL (solid lines) and inverted TL (dashed lines) from the best model at 250 Hz for both the 20- and 85-m deep array (the TL at 85 m has been offset downward 25 dB). Note that data from this frequency have not been used in the inversion and is, thus, a test of how well the inversion ran. *(left, lower middle)* The match of the data (solid lines) and inverted field (dashed lines) on the vertical array at the same frequencies (50 and 300 Hz) as used in the inversion. *(bottom)* The obtained (dashed lines) and

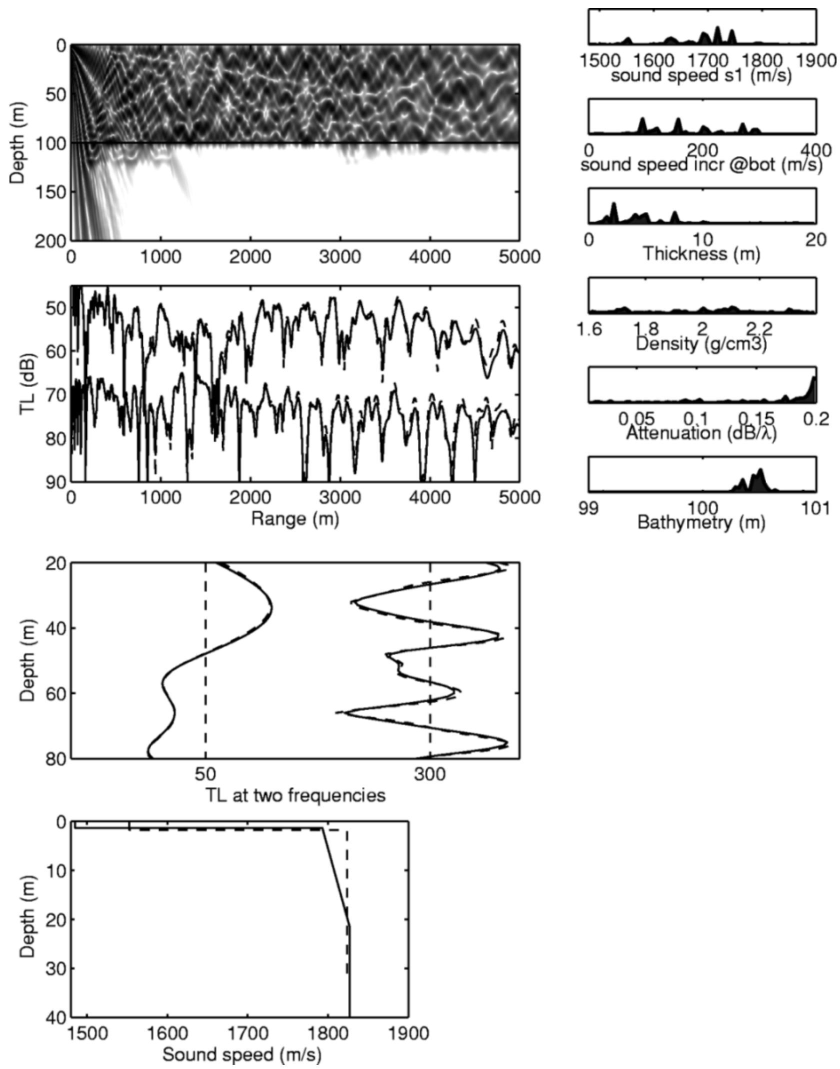

Fig. 16. Inversion display for TC3 using vertical array data at 2.5 km. The parameter estimates refers here to the intrusion.

true (solid lines) velocity profile; the true profile was supplied after the workshop. *(right)* The *a posteriori* distributions.

For estimating the *posteriori* distribution, the effective number of propagating modes N_e must be estimated. Using a covariance matrix for the VLA data, averaged over the ten ranges 0.5–5 km, N_e was found to vary from 2 to 4 between 50 and 200 Hz [32]. We chose to use a constant value $N_e = 3$. For transmission-loss inversion, the effective number of hydrophones are larger due to range dependence of the field; we use $N_e = 6$.

For TC1 and TC2, results are shown for inversion from the vertical array at 0.5 km (Figs. 5 and 7) and 3-km (Figs. 6 and 8) range and for transmission loss (Figs. 9 and 10). For transmission loss, data over 0.1–3 km range were used.

From the figures, we observe the following.

- The first sediment layer thickness is always well determined.
- The sound speed is, in general, much better determined close to the surface than deeper in the sediment. This is natural, as the wave propagation is more influenced by the shallower sediments.
- The transmission-loss plots (*left, upper middle*) are very useful in assessing the solution. For example, because low-order modes penetrate deeper than high-order modes, a mismatch in low-order modes indicates that the deeper sediments are not matched well and a high-order mode mismatch indicates that the upper sediments are not matched well.
- The TL mismatch for the data not used in the inversion (*left, upper middle*) in Fig. 9 indicates that the low-order modes are not matched well. These modes penetrate deeper into the sediment, which indicates a sound speed mismatch somewhat deeper in the sediment.
- TL inversions, Figs. 9 and 10, seem to give comparable results to the VA inversions, Figs. 5–16.

Finally, the parameter estimates corresponding to the best fitness for all of the test cases are summarized in Table II.

III. Phenomenological Inversion of TC3

For this test case, we were informed that there was an intrusion in the bottom. Three methods for locating the intrusion were investigated as follows:

TABLE II
GA PARAMETER ESTIMATES FOR TC1–TC3 FOR DATA FROM THE VERTICAL ARRAY AT 0.5 AND 3 KM AND FROM TL. FOR TC3 , THE "VA 0.5 KM" REFERS TO VALUES IN THE FIRST AND THIRD SECTOR (0–1.1 KM AND 2.9–5 KM) AND "VA 2.5 KM" REFERS TO THE SECOND SECTOR (1.1–2.9 KM)

Model parameter	TC1 VA 0.5km	TC1 VA 3km	TC1 TL	TC2 VA 0.5km	TC2 VA 3 km	TC2 TL	TC3 VA 0.5km
Objective function	0.0083	0.0065	0.00042	0.0181	0.0129	0.00027	0.0061
Sediment							
sound speed, c_1 (m/s)	1506	1523	1492	1555	1551	1563	1495
sound speed, c_2 (m/s)	1738	1767	1722	1587	1562	1564	1620
sound speed, c_3 (m/s)	1761	1791	1811	1600	1620	1648	1749
thickness, h_1 (m)	4.1	4.5	4.1	8.6	1.0	4.5	4.1
thickness, h_2 (m)	3.4	12.8	8.9	4.4	8.2	8.6	3.4
thickness, h_3 (m)	18.6	24.5	13.3	4.8	12.8	5.8	18.6
attenuation (dB/λ)	0.24	0.17	0.38	0.07	0.28	0.21	0.49
density (g/cm^3)	1.67	1.8	1.7	1.48	1.67	1.70	1.78
Bottom							
sound speed, c_b (m/s)	2121	2126	1855	1840	1924	1854	1826
attenuation (dB/λ)	0.02	0.18	0.09	0.167	0.07	0.07	0.16
density (g/cm^3)	1.64	2.1	2.4	1.95	1.74	2.4	1.75

- transmission loss;
- back propagation;
- plane wave beamforming.

The transmission loss and back propagation require modeling using a range-independent environment. Using the environmental model in Section II and inverting the vertical array data at 500-m range gives the reference environment used in this section (see Fig. 11 and Table II).

A. Transmission Loss

This is the simplest approach. The frequency-averaged transmission loss along the 85-m deep horizontal array very clearly shows the start and end of the intrusion (see Fig. 12). In order to limit the dynamic range, the transmission loss is corrected for cylindrical spreading by multiplying with range [adding $10\log(R)$]. The structure of the TL curve indicates that a harder material is present from 1100 to 2900 m, which is especially evident in the TL for the low-frequency 25–50 Hz, data (solid line).

It is not clear how close the intrusion is to the surface. To investigate this, the intrusion is modeled with no sediment [Fig. 13(a)] and with a 10-m thick sediment [Fig. 13(b)]. The bottom environment for this model was determined based on a bottom inversion of the data at the array at 500-m range. The same environment as the basement for the 0–1100-m sector is used in the sector with the intrusion. Based on this simple modeling, it is concluded that the basement is close to the sea-bed interface. The precise thickness will be determined using optimization (see Section II).

B. Back Propagation

Using a simple time-reverse approach, as described in [36], the phase conjugate of the signals received at the vertical receive array are submitted as sources. Geoacoustic inversion using back propagation has been described by Dizaji *et al.* [37]. If the same environment is used for the forward and backward propagation and the array aperture is sufficiently large, then the field should refocus at the source. When there are inhomogeneities in the forward environment, the backward field should also focus on the interfaces of the inhomogeneity. This follows from Green's theorem (see e.g., [38]). The bottom environment for this model was determined based on a bottom inversion of the data at the array at 500-m range. The back propagation was done using the data from each of the nine vertical arrays from 1–5-km ranges, as shown in Fig. 14. In the water column, several peaks are seen due to ambiguities. Only close to the array does the field interact significantly with the bottom. Thus, the changes in the environment are seen only when using the array at 1.5- and 3-km range.

C. Plane Wave Beamforming

A simple configuration would be to have a ship sailing over the intrusion towing a horizontal array and a source [39]. In such a configuration, it would be possible to determine geoacoustic parameters. Lacking such a configuration, the complex-valued horizontal pressure at 85-m depth is used to simulate a 200-m long array. The beam response as a function of range from the source to start of the array and grazing angle (90° is downward looking) is shown in Fig. 15. The major part of this response is dominated by the waveguide interference, occurring at regular intervals in both angle and range. When passing over an inhomogeneity in the bottom, the pressure field and, thus, the beam response will change. This is seen as vertical lines in the range-angle plot (Fig. 15).

The most drastic field changes are seen when scattering off a harder material. Thus, the plane wave beamforming, Fig. 15, is best at detecting the vertical interface at 1.1-km range (the

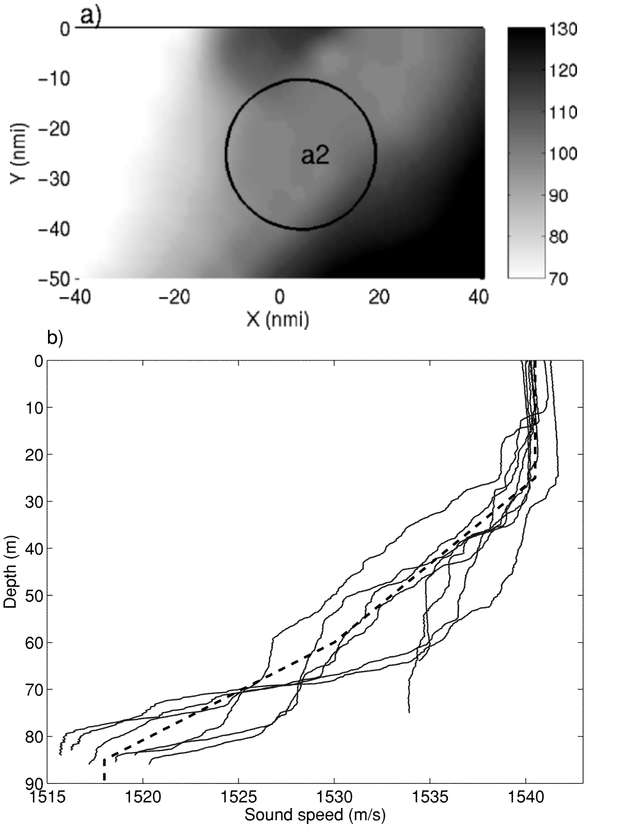

Fig. 17. Environment for TC4 (East China Sea). (a) Bathymetry (m) map and (b) measured (solid line) and approximated (dashed line) sound speed profiles.

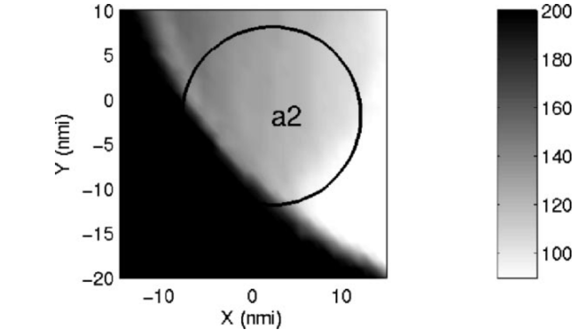

(a)

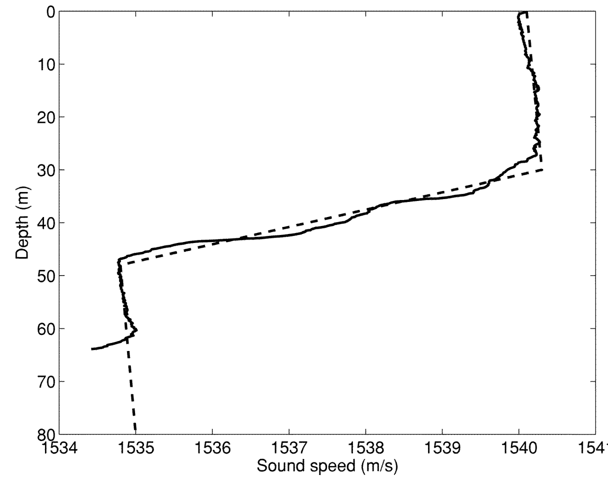

(b)

Fig. 18. Environment for TC5 (Gulf of Mexico). (a) Bathymetry (m) and (b) measured (solid line) and approximated (dashed line) sound speed.

source is radiating from 0 range toward the harder intrusion). In contrast, the back propagation, Fig. 14, best detects the vertical interface at 2.9-km range (the back propagating source is radiating from 3 km toward the harder intrusion).

D. *Inversion of Intrusion Sector*

In Sections III-A–C, we have found the range of the intrusion (1.1–2.9 km) and determined the parameters outside the intrusion (see Fig. 11). Now an inversion to find the depth of the intrusion and the environmental properties is carried out (see Fig. 16 and Table II). In this inversion, the properties from the inversion at 500-m range is used in the first 0–1.1 km. The intrusion is assumed to be of homogeneous material and for the layer above the intrusion we only invert for the sound speed and thickness.

IV. Reverberation Test Cases (TC4 and TC5)

Two real-data test cases also were supplied. For this test, drifting sonobuoys dropped from airplanes were used for data in the East China Sea (TC4) and the Gulf of Mexico (TC5). Both incoherent transmission-loss data and reverberation data were supplied. While SAGA can handle both types of data, we chose to focus on the reverberation data using the same approach, as described in Ellis and Gerstoft [40]. For simplicity, data from only one shot were used. Ideally, data from neighboring shots should be used to obtain a more robust signal estimate. The reverberation inversions were run using the POPP normal mode reverberation code [10] and a simple Lambert scattering strength was computed for each frequency. The environment was assumed range independent and the ocean sound speed profile was obtained from measurements. The inversion effort was split evenly between estimating scattering parameters and bottom parameters. The following parameters were estimated: five Lambert scattering strengths (one for each frequency); average bathymetry; the sound speed at 0, 5, 20 m depth (with linear variation between these points); and attenuation. This involved minor work as a case from [40] was used. There were 5000 forward models evaluated in the optimization. The replica and data were compared using a least squares objective function.

The bathymetry (top) and sound speed profile (bottom) for TC4 and TC5 are shown in Figs. 17 and 18, respectively. The sonobouys are located in the center of the circles (a2) and the radius indicates the maximum propagation distance in the time interval used for the inversion. The bathymetry for TC5 is slightly more range dependent than for TC4. In both cases, visual approximation (dashed line) to the observed sound speed profiles were used in the inversions.

The data are shown in Figs. 19 and 20 (gray). As the source and receiver are relatively close, a monostatic model can be used a few seconds after the main blast. The noise level before the blast is indicated by the solid horizontal line. The data from a few seconds after the blast until it reaches the noise floor is used in the inversion; the time interval is indicated by dotted vertical

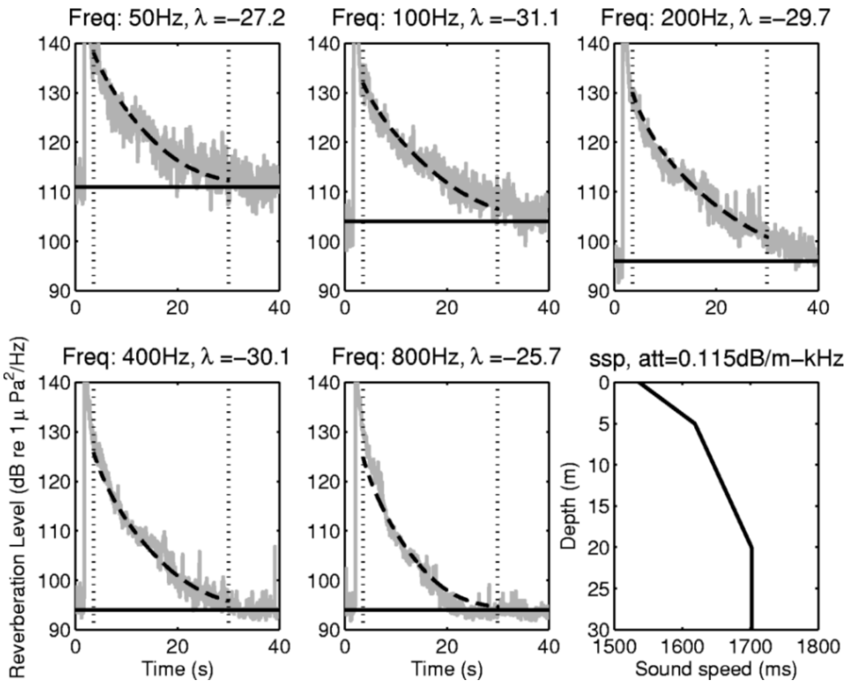

Fig. 19. Reverberation data (gray area) and estimated match (dashed line) for TC4 for 50, 100, 200, 400, and 800 Hz. The solid horizontal line indicates the estimated noise floor and the two vertical lines the range of data used for the inversion. The estimated Lambert scattering strength is indicated on top of each plot. The last plot shows the estimated geoacoustic profile.

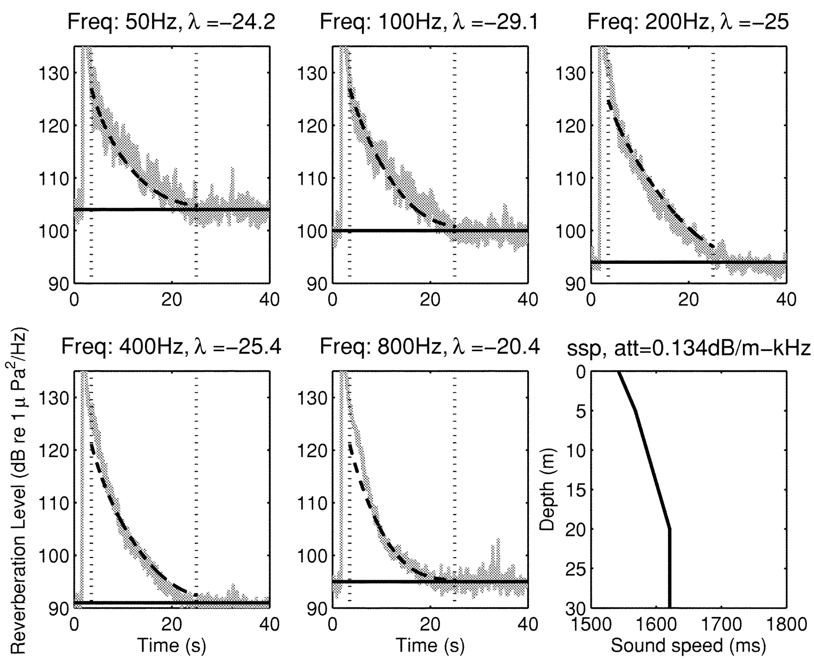

Fig. 20. Reverberation data (gray area) and estimated match (dashed line) for TC5 for 50, 100, 200, 400, and 800 Hz. The solid horizontal line indicates the estimated noise floor and the two vertical lines the range of data used for the inversion. The estimated Lambert scattering strength is indicated on top of each plot. The last plot shows the estimated geoacoustic profile.

lines. The best match to the reverberation is shown as the dashed lines in Figs. 19 and 20.

The estimated Lambert scattering coefficients are indicated in the plot for each frequency. For TC4, these are close to the classical Lambert coefficient of -27 dB. Whereas for TC5, these are about 5 dB higher, indicating that the scattering in the TC5 region is relatively stronger. For both regions, the scattering coefficients tend to increase with frequency, which is reasonable as the scattering normally increases with frequency.

The rate of decay of the reverberation curve is determined by the bottom loss (increase in sound speed and decrease in attenuation yields a slower decay). From Figs. 19 and 20, the reverberation rate of decay is seen to be faster for TC5 than TC4. In agreement with this, the sound speed estimate is higher and the attenuation estimate lower for TC4 than TC5.

This type of data does not contain as much information as multifrequency complex-valued array data commonly used in matched field inversions and supplied in TC1–TC3. Thus, the results of the inversion are more uncertain. Essentially, the data can be described by an offset and a slope for each frequency. For a total of five frequency bands, this gives about ten parameters, (we used nine parameters in the present inversion). The five Lambert coefficients determine the offset at each frequency, the attenuation influences a frequency dependent slope, andthe bottom sound speed profile (three parameters) influences both the offset and the slope. Thus, the parameters used in the inversion are expected to be reasonably independent.

V. Conclusion

The inverse problem is difficult to solve and requires cooperation between many neighboring fields. An understanding of the physical problem is important and the effort to do this should be done before an inversion is carried out. The inversion here is carried out as a multiparameter optimization problem. Inspecting the physical correctness of the solution and the uncertainty is important in the assessment of the solution.

For these inversions, the SAGA code was used. This enabled us to easily assess the quality of our inversion. Here, the approach has been applied to complex-valued vertical array data, transmission-loss data, and reverberation data. For detection of the intrusion, we investigated three methods: transmission loss, back propagation, and plane wave beamforming. For the present case, using frequency-averaged transmission loss gave the best results. Which method is most advantageous likely is strongly case dependent and all methods appear to be useful.

References

[1] N. R. Chapman, S. Chin-Bing, D. King, and R. B. Evans, "Benchmarking geoacoustic inversion methods for range-dependent waveguides," *IEEE J. Oceanic Eng.*, vol. 28, pp. 320–330, July 2003.

[2] M. D. Collins, "A split-step Padé solution for parabolic equation method," *J. Acoust. Soc. Amer.*, vol. 93, pp. 1736–1742, 1993.

[3] P. Gerstoft and D. F. Gingras, "Parameter estimation using multi-frequency range-dependent acoustic data in shallow water," *J. Acoust. Soc. Amer.*, vol. 99, pp. 2839–2850, 1996.

[4] P. M. van den Berg and R. E. Kleinman, "A contrast source inversion method," *Inverse Problems*, vol. 13, pp. 1607–20, 1997.

[5] M. Lambert and D. Lesselier, "Binary-constrained inversion of buried cylindrical obstacle from complete and phaseless magnetic fields," *Inverse Problems*, vol. 16, pp. 563–576, 1998.

[6] P. Gerstoft. (1997) SAGA Users Guide 2.0. SACLANT Undersea Research Centre, La Spezia, Italy. [Online]. Available: http://www.mpl.ucsd.edu/people/gerstoft/saga

[7] ——, "Inversion of seismoacoustic data using genetic algorithms and a posteriori probability distributions," *J. Acoust. Soc. Amer.*, vol. 95, no. 2, pp. 770–782, 1994.

[8] F. B. Jensen and M. C. Ferla, "SNAP-The SACLANTCEN Normal Mode Acoustic Propagation Model," SACLANT Undersea Research Centre, La Spezia, Italy, SM-121, 1979.

[9] H. Schmidt, "SAFARI: Seismo-Acoustic Fast Field Algorithm for Range Independent Environments. User's guide," SACLANT Undersea Research Centre, La Spezia, Italy, SR-113, 1987.

[10] D. D. Ellis, "A shallow water normal mode reverberation model," *J. Acoust. Soc. Amer.*, vol. 97, no. 5, pp. 2804–2814, 1995.

[11] F. Bini-Verona, P. L. Nielsen, and F. B. Jensen, "PROSIM Broadband Normal-Mode Model: A User's Guide," SACLANT Undersea Research Centre, La Spezia, Italy, SM-358, 1999.

[12] E. K. Westwood, C. T. Tindle, and N. R. Chapman, "A normal mode model for acousto-elastic ocean environments," *J. Acoust. Soc. Amer.*, vol. 100, no. 6, pp. 3631–3645, 1996.

[13] E. K. Westwood and P. J. Vidmar, "Eigenray finding and time series simulation in a layered bottom ocean," *J. Acoust. Soc. Amer.*, vol. 81, no. 4, pp. 912–924, 1987.

[14] A. E. Barrios, "A terrain parabolic equation model for propagation in the troposphere," *IEEE Trans. Antennas Propagat.*, vol. 42, pp. 90–98, Jan. 1994.

[15] M. I. Taroudakis and M. G. Markaki, "Bottom geoacoustic inversion by "broadband" matched field processing," *J. Comput. Acoust.*, vol. 16, no. 2, pp. 167–183, 1998.

[16] M. D. Collins, W. A. Kuperman, and H. Schmidt, "Nonlinear inversion for ocean-bottom properties," *J. Acoust. Soc. Amer.*, vol. 92, no. 5, pp. 2770–2783, 1992.

[17] C. E. Lindsay and N. R. Chapman, "Matched field inversion for geophysical parameters using adaptive simulated annealing," *IEEE J. Oceanic Eng.*, vol. 18, pp. 224–231, July 1993.

[18] S. E. Dosso, M. L. Yeremy, J. M. Ozard, and N. R. Chapman, "Estimation of ocean bottom properties by matched-field inversion of acoustic field data," *IEEE J. Oceanic Eng.*, vol. 18, pp. 232–239, July 1993.

[19] M. D. Collins and L. Fishman, "Efficient navigation of parameter landscapes," *J. Acoust. Soc. Amer.*, vol. 98, no. 3, pp. 1637–1644, 1995.

[20] W. Seong and C. Park, "The fine scale geoacoustic inversion of the shallow water sub-bottom using chirp sonar," *Proc. IEEE Oceans*, pp. 723–730, 2001.

[21] M. Snellen and D. G. Simons, "Application of a downhill simplex algorithm to reduce the uncertainty in matched field inversion results," *J. Acoust. Soc. Amer.*, submitted for publication.

[22] P. Gerstoft, "Inversion of acoustic data using a combination of genetic algorithms and the Gauss–Newton approach," *J. Acoust. Soc. Amer.*, vol. 97, no. 4, pp. 2181–2191, 1995.

[23] G. R. Potty, J. H. Miller, J. F. Lynch, and K. B. Smith, "Tomographic inversion for sediment parameters in shallow water," *J. Acoust. Soc. Amer.*, vol. 108, no. 3, pp. 973–986, 2000.

[24] M. R. Fallat and S. E. Dosso, "Geoacoustic inversion via local global and hybrid algorithms," *J. Acoust. Soc. Amer.*, vol. 105, no. 6, pp. 3219–3230, 1999.

[25] M. Musil, M. J. Wilmut, and N. R. Chapman, "A hybrid simplex genetic algorithm for estimating geoacoustic parameters using matched field inversion," *IEEE J. Oceanic Eng.*, vol. 24, pp. 358–369, July 1999.

[26] S. E. Dosso, M. J. Wilmut, and A.-L. S. Lapinski, "An adaptive-hybrid algorithm for geoacoustic inversion," *IEEE J. Oceanic Eng.*, vol. 26, pp. 324–336, July 2001.

[27] P. Gerstoft and C. F. Mecklenbräuker, "Ocean acoustic inversion with estimation of a posteriori probability distributions," *J. Acoust. Soc. Amer.*, vol. 104, no. 2, pp. 808–817, 1998.

[28] C. F. Mecklenbräuker and P. Gerstoft, "Objective functions for ocean acoustic inversions derived by likelihood methods," *J. Comput. Acoust.*, vol. 8, no. 2, pp. 259–270, 2000.

[29] S. E. Dosso and P. L. Nielsen, "Quantifying uncertainties in geoacoustic inversion: II Application to broadband, shallow water data," *J. Acoust. Soc. Amer.*, vol. 111, no. 1, pp. 143–159, 2002.

[30] E. L. Hamilton, "Geoacoustic modeling of the sea floor," *J. Acoust. Soc. Amer.*, vol. 68, no. 5, pp. 1313–40, 1980.

[31] S. E. Dosso, "Quantifying uncertainties in geoacoustic inversion. I a fast gibbs sampler approach," *J. Acoust. Soc. Amer.*, vol. 111, no. 1, pp. 129–142, 2002.

[32] C. A. Gillard, D. J. Thompson, and G. J. Heard, "Estimating geoacoustic parameters using matched-field inversion methods," *IEEE J. Oceanic Eng.*, vol. 28, July 2003.

[33] G. L. D'Spain, J. J. Murray, W. S. Hodgkiss, N. O. Booth, and P. W. Schey, "Mirages in shallow water matched field processing," *J. Acoust. Soc. Amer.*, vol. 105, no. 6, pp. 3245–3265, 1999.

[34] C. F. Mecklenbräuker, P. Gerstoft, J. F. Böhme, and P.-J. Chung, "Hypothesis testing for acoustic environmental models using likelihood ratio," *J. Acoust. Soc. Amer*, vol. 105, no. 3, pp. 1738–1748, 1999.

[35] P. L. Nielsen, M. Siderius, and P. Gerstoft, "Range-dependent geoacoustic inversion: Results from the inversion techniques workshop," *IEEE J. Oceanic Eng.*, vol. 28, pp. 414–423, July 2003.

[36] W. A. Kuperman, W. S. Hodgkiss, H. C. Song, T. Akal, C. Ferla, and D. R. Jackson, "Phase conjugation in the ocean: Experimental demonstration of an time reversed mirror," *J. Acoust. Soc. Amer.*, vol. 102, no. 1, pp. 1–16, 1997.

[37] R. M. Dizaji, N. R. Chapman, and R. L. Kirlin, "A phase regulated propagation technique for geoacoustic inversion," *J. Acoust. Soc. Amer.*, vol. 111, no. 2, pp. 800–808, 2002.

[38] F. B. Jensen, W. A. Kuperman, M. B. Porter, and H. Schmidt, *Computational Ocean Acoustics*. New York: Springer Verlag, 1994.

[39] M. Siderius, P. Nielsen, and P. Gerstoft, "Range-dependent seabed characterization by inversion of acoustic data from a towed receiver array," *J. Acoust. Soc. Amer.*, vol. 112, no. 4, 2002.

[40] D. D. Ellis and P. Gerstoft, "Using inversion techniques to extract bottom scattering strengths and sound speed from shallow water reverberation data," in *Proc. Third European Conf. Underwater Acoust.*, J. Papadakis, Ed., Crete, Greece, 1996, pp. 887–892.

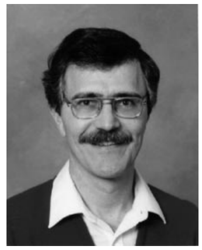

William S. Hodgkiss (S'68–M'75) was born in Bellefonte, PA, on August 20, 1950. He received the B.S.E.E. degree from Bucknell University, Lewisburg, PA, in 1972 and the M.S. and Ph.D. degrees in electrical engineering from Duke University, Durham, NC, in 1973 and 1975, respectively.

From 1975 to 1977, he was with the Naval Ocean Systems Center, San Diego, CA. From 1977 to 1978, he was a Faculty Member in the Electrical Engineering Department, Bucknell University. Since 1978, he has been a Member of the Faculty, Scripps Institution of Oceanography, University of California, San Diego, and on the staff of the Marine Physical Laboratory, where he is currently Deputy Director. His present research interests are in the areas of adaptive array processing, propagation modeling, and environmental inversions with applications of these to underwater acoustics and electromagnetic wave propagation.

Dr. Hodgkiss is a Fellow of the Acoustical Society of America.

William A. Kuperman has conducted theoretical and experimental research in ocean acoustics and signal processing at the Naval Research Laboratory, SACLANT Undersea Research Centre, La Spezia, Italy, and at the Scripps Institution of Oceanography (SIO), University of California, San Diego.

He currently is a Professor at SIO and the Director of its Marine Physical Laboratory.

Peter Gerstoft (M'03) received the M.Sc. and Ph.D. degrees from the Technical University of Denmark, Lyngby, in 1983 and 1986, respectively, and the M.Sc. degree from the University of Western Ontario, London, ON, Canada, in 1984.

From 1987 to 1992, he was with Ødegaard and Danneskiold-Samsøe, Copenhagen, Denmark, working on forward modeling and inversion for seismic exploration, with a year as Visiting Scientist at the Massachusetts Institute of Technology, Cambridge. From 1992 to 1997, he was Senior Scientist at SACLANT Undersea Research Centre, La Spezia, Italy, where he developed the SAGA inversion code, which is used for ocean acoustic and electromagnetic signals. Since 1997, he has been with the Marine Physical Laboratory, University of California, San Diego. His research interests include global optimization; modeling; and inversion of acoustic, elastic, and electromagnetic signals.

Heechun Song (M'02) received the B.S. and M.S. degrees in marine engineering and naval architecture from Seoul National University, Seoul, Korea, in 1978 and 1980, respectively, and the Ph.D. degree in ocean engineering from the Massachusetts Institute of Technology, Cambridge, in 1990.

From 1991 to 1995, he was with Korea Ocean Research and Development Institute, Ansan. Since 1996, he has been a Member of the Scientists of the Marine Physical Laboratory/Scripps Institution of Oceanography, University of California, San Diego. His research interests include time-reversed acoustics, robust matched-field processing, and wave-propagation physics.

Dr. Song is a Fellow of the Acoustical Society of America.